Chlorination Chemistry. 3. Ab Initio Study of the Reaction of Chlorine Atom with Allene

Jeffrey W. Hudgens*,† and Carlos Gonzalez*,‡

Physical and Chemical Properties Division, Chemical Science and Technology Laboratory, National Institute of Standards and Technology, Gaithersburg, Maryland 20899

Received: October 17, 2001; In Final Form: December 27, 2001

Highly correlated ab initio molecular orbital calculations have been used to map out the potential energy surface of the Cl + allene reaction in the gas phase. Eight transition state structures governing the mechanism of the title reaction were computed at seven different levels of theory. The results show that UMP2 calculations are adversely affected by contamination from higher spin states. QCISD(T) calculations illustrate the importance of correlation including triple electron excitations in the quadratic configuration wave function for obtaining an accurate description of the potential energy surface. Results computed at the QCISD(T)/6-31+G(d,p)// QCISD/6-31+G(d,p) level indicate that chlorine atom addition at the center and end carbons of allene are barrierless processes and that the chemically activated C_3H_4Cl complex may isomerize through chlorine atom transfer but not through hydrogen atom transfer. The metathesis transition state corresponding to hydrogen abstraction by chlorine lies 15 $kJ{\cdot}mol^{-1}$ above reactants. The isomerization reaction path between the 3-chloro-1-propen-2-yl and 2-chloroallyl radical adducts lies below the initial reactants, permitting the incipient C_3H_4-Cl ensembles to establish equilibrium. Thus, the dominant addition product of Cl + allene is the 2-chloroallyl radical.

Introduction

Gas-phase reactions of chlorine with hydrocarbons play important roles during the synthesis of chlorinated compounds in a variety of environments. Consequently, knowledge of their elementary reaction rate coefficients and mechanisms is important for accurate models of industrial manufacturing and waste incineration. Although the kinetic rate equations of C1−C4 alkanes, ethylene, and propene are well represented in the kinetics literature,[1] the few rate coefficient measurements of chlorine reacting with the simple C3 unsaturated species, allene and propyne, span a limited set of physical conditions.[2−4] The understanding of the governing reaction mechanism is also incomplete.[3,4] More extensive rate coefficient data, extending to high pressures and temperatures, may become important to future models of incineration processes. Under conditions characterized by incomplete mixing, Tsang has suggested that the pyrolysis of organic waste may produce unsaturated hydrocarbons, including allene, that subsequently react with the chlorine atoms liberated by the oxidation of chlorinated species. Subsequent reactions of these chlorinated organic products may feed reaction sequences that produce an undesirable, highly chlorinated, inert effluent from incinerators.[5] In an earlier paper we reported rate coefficient measurements observed in the Cl + allene system at 298 K, estimated thermochemical properties of relevant chlorinated products, and proposed a mechanism for the Cl + allene reaction.[4] This paper refines our understanding of the Cl + allene reaction mechanism by describing the ab initio results of the governing transition state structures. The ab initio data provide a starting point for future estimates of the high pressure and temperature rate coefficients of Cl + allene by use of master rate equation methods.[6]

† E-mail: jeffrey.hudgens@nist.gov.
‡ E-mail: carlos.gonzalez@nist.gov.

The Cl atom may react with allene through metathesis and addition channels,

$$H_2C{=}C{=}CH_2 + {}^{\bullet}Cl$$

$$\rightarrow HCl + {}^{\bullet}C_3H_3 \qquad \Delta_{rxn}H^{\circ}_{298.15} = -63 \pm 7\ kJ{\cdot}mol^{-1} \quad (1)$$

$$\rightarrow CH_2Cl\text{-}\dot{C}{=}CH_2 \qquad \Delta_{rxn}H^{\circ}_{298.15} = -71 \pm 7\ kJ{\cdot}mol^{-1} \quad (2)$$

$$\rightarrow {}^{\bullet}\left[CH_2 \overset{..}{-} CCl \overset{....}{-} CH_2\right] \qquad \Delta_{rxn}H^{\circ}_{298.15} = -170 \pm 9\ kJ{\cdot}mol^{-1} \quad (3)$$

where reaction **1** produces the resonance-stabilized propargyl radical and reactions **2** and **3** form the 3-chloro-1-propen-2-yl radical and the 2-chloroallyl radical by chlorine atom addition at the end and center carbons, respectively. Using an infrared diode laser, Farrell and Taatjes [3] measured the HCl metathesis yield of reaction **1** between 295 and 1100 K. At 300 K they found that chlorine addition accounts for ≈98% of the total reaction. They found that the fractional metathesis yield increased with temperature. Above 800 K metathesis accounts for all of the reaction. We studied Cl + allene using a cavity ring-down spectroscopy apparatus that can sensitively detect the ultraviolet absorptions of the C_3H_4Cl radical adduct and of the propargyl radical.[4,7−9] At 298 K the 332.5 nm absorption band of the propargyl radical was below the apparatus detection threshold, indicating that reaction **1** was negligible. The C_3H_4-Cl adduct produced strong absorption signals at 242 nm, enabling determinations of $k(Cl + C_3H_4)$, and $k(C_3H_4Cl + C_3H_4Cl)$ and $k(C_3H_4Cl + O_2)$.[4]

Because chlorine addition to allene may produce two or more C_3H_4Cl isomers, these rate coefficients are of limited value to modeling unless the dominant C_3H_4Cl isomer product is

10.1021/jp013862a Published 2002 by the American Chemical Society
Published on Web 02/02/2002

assigned. Thermochemistry favors reaction **3** because the 2-chloroallyl radical is 100 kJ·mol^{-1} more stable than the 3-chloro-1-propen-2-yl radical. However, end-product experiments of allene with radicals do not support a simple mechanism based on radical stability. End-product analyses of radical addition reactions, R−S$^{\bullet}$ + allene and $^{\bullet}CF_3$ + allene, found products formed mainly by radical addition to the end carbon,[10,11] suggesting that the dominant gas-phase adducts are substituted vinyl-like radicals. But end-product analyses of Br + allene found the newly added halogen atoms on the center carbon, suggesting that the persistent gas-phase adduct radical is the more stable 2-bromoallyl radical.[12,13] These results do not rule out a third mechanism involving radical addition to both carbon sites on allene, followed by isomerization to the favored product.

Reactions **2** and **3** form incipient ensembles of 3-chloro-1-propen-2-yl and 2-chloroallyl radicals. Since both radicals are chemically activated, containing internal energy equal to their reaction exothermicity, we consider the isomerization channels involving transfer of a chlorine or hydrogen atom. The 3-chloro-1-propen-2-yl radical may isomerize, forming the 2-chloroallyl radical through a 3,2-chlorine transfer, e.g.,

$$CH_2Cl{-}\dot{C}{=}CH_2 \xrightarrow{3,2\text{-Cl}} {}^{\bullet}\left[CH_2\cdots CCl\cdots CH_2\right] \qquad \Delta_{rxn}H^{\circ}_{298.15} = -99 \pm 9\ \text{kJ·mol}^{-1} \quad (4)$$

A 3,2-hydrogen atom transfer in the 3-chloro-1-propen-2-yl radical will form the 1-chloroallyl radical

$$CH_2Cl{-}\dot{C}{=}CH_2 \xrightarrow{3,2\text{-H}} {}^{\bullet}\left[CHCl\cdots CH\cdots CH_2\right] \qquad \Delta_{rxn}H^{\circ}_{298.15} = -101 \pm 9\ \text{kJ·mol}^{-1} \quad (5)$$

and a 3,1-hydrogen atom transfer will form 1-chloro-1-propen-2-yl:

$$CH_2Cl{-}\dot{C}{=}CH_2 \xrightarrow{3,1\text{-H}} CHCl{=}\dot{C}{-}CH_3 \qquad \Delta_{rxn}H^{\circ}_{298.15} = -8 \pm 5\ \text{kJ·mol}^{-1} \quad (6)$$

At low pressures the 1-chloroallyl radical formed by reaction **5** will initially contain ≈170 kJ·mol^{-1} internal energy. So, we also consider isomerization of 1-chloroallyl into the 1-chloro-1-propen-2-yl radical through a 2,3-hydrogen transfer:

$${}^{\bullet}\left[CHCl\cdots CH\cdots CH_2\right] \xrightarrow{2,3\text{-H}} CHCl{=}\dot{C}{-}CH_3 \qquad \Delta_{rxn}H^{\circ}_{298.15} = +95 \pm 8\ \text{kJ·mol}^{-1} \quad (7)$$

Finally, we consider a reaction scheme composed of three elementary isomerization reactions that transforms the 2-chloroallyl radical into the 1-chloroallyl radical:

$${}^{\bullet}\left[CH_2\cdots CCl\cdots CH_2\right] \xrightarrow{1,3\text{-H}} \dot{C}H{=}CCl{-}CH_3 \qquad \Delta_{rxn}H^{\circ}_{298.15} = +91 \pm 15\ \text{kJ·mol}^{-1} \quad (8)$$

$$\dot{C}H{=}CCl{-}CH_3 \xrightarrow{2,1\text{-Cl}} CHCl{=}\dot{C}{-}CH_3 \qquad \Delta_{rxn}H^{\circ}_{298.15} = +0 \pm 7\ \text{kJ·mol}^{-1} \quad (9)$$

$$CHCl{=}\dot{C}{-}CH_3 \xrightarrow{3,2\text{-H}} {}^{\bullet}\left[CHCl\cdots CH\cdots CH_2\right] \qquad \Delta_{rxn}H^{\circ}_{298.15} = -99 \pm 8\ \text{kJ·mol}^{-1} \quad (10)$$

Although reaction **8** is very endothermic, the internal energy contained by chemically activated 2-chloroallyl radicals may be expected to fulfill the enthalpy requirement.

Computational Methods and Terminology

All calculations[14] described herein were carried out with the Gaussian 94 and Gaussian 98 program suites[15,16] on a Cray C90/6256 super-computer and a 32-processor Silicon Graphics Origin 2000 parallel computer. Fully optimized geometries of reactants, intermediates (designated with "IS" prefixes), transition structures (designated with "TS" prefixes), and products, were computed with the unrestricted second-order Møller−Plesset perturbation theory (UMP2),[17] the hybrid gradient corrected three-parameter B3LYP density functional theory,[18] and the quadratic configuration interaction (QCISD) level,[19] including single and double electronic excitations. All calculations were carried out using the 6-31+(d,p) basis set.[20−24] In this work, we follow the standard notation "Theory/basis" to indicate that a full geometry optimization has been carried out at the "Theory" level using the "basis" basis set. In addition, the terms "Theory2/basis2//Theory1/basis1" are used to indicate a single point energy calculation at the "Theory2/basis2" level of theory using the geometry previously optimized at the "Theory1/basis1" level. H^{MP2}, H^{B3LYP}, and H^{QCISD} denote the electronic energies of the fully optimized structures obtained at the MP2/6-31+G(d,p), B3LYP/6-31+(d,p), and QCISD/6-31+G(d,p) levels, respectively. H^{PMP2} denotes the MP2 electronic energy computed at the fully optimized MP2/6-31+G(d,p) geometry after full annihilation of the spin contaminants using the method of Schlegel.[25−28] For each fully optimized MP2, B3LYP, and QCISD geometry, we performed single point calculations with the 6-311+G(d,p) basis at the quadratic configuration interaction level, including single and double electron excitations and a perturbative correction for triple excitations (i.e., QCISD(T)/6-311+G(d,p)). The electronic energies obtained from these calculations are denoted $H^{Q(T)//MP2}$, $H^{Q(T)//B3LYP}$, and $H^{Q(T)//QCISD}$, respectively. Reaction pathways were computed by the IRC algorithm of Gonzalez and Schlegel,[29−31] as implemented in the G94 and G98 program suites. Harmonic vibrational frequencies and zero point energy corrections, $(H_0^{ZPE})^{level}$, were computed at the MP2/6-31+G(d,p), B3LYP/6-31+(d,p), and QCISD/6-31+(d,p) levels. All computational results, presented herein, contain no empirical scaling of vibrational frequencies or zero point energies.

In some figures we plot $\Delta_{path}H^{level}$, the electronic energy of the IRC reaction path relative to the electronic energies of allene and the chlorine atom. We note that $\Delta_{path}H^{level}$ does not include zero point energy contributions. When zero point energy is accounted at the stationary points, we quote $\Delta_{rel}H_0^{level}$, the energy at 0 K of a stationary point relative to the initial reactants. For example,

$$\Delta_{rel}H_0^{Q(T)//MP2}(TS) = H_0^{Q(T)//MP2}(TS) - H_0^{Q(T)//MP2}(\text{allene}) - H_0^{Q(T)//MP2} \quad (C1)$$

where $H_0^{Q(T)//MP2} = H^{Q(T)//MP2} + (H_0^{ZPE})^{MP2}$. One table also reports $\Delta_{rel}H_0^{PMP2}$ which was computed using $H_0^{PMP2} = H^{PMP2} + (H_0^{ZPE})^{MP2}$.

Results

Thermochemical Properties and Geometry Parameters. For each stable molecule and persistent radical found in reactions **1**−**10** Table 1 lists $H^{Q(T)//QCISD}$, the electronic energy,

TABLE 1: Ab Initio Results and Thermochemical Data Used to Estimate Relative Energies of Species Involved in the Cl + Allene System

species	$H^{Q(T)/QCISD}$, hartree[a]	$(H_0^{ZPE})^{MP2}$, hartree[a]	$\Delta_f H_0^\circ$,[b] kJ mol^{-1}	$\Delta_f H_{298.15}^\circ$,[b] kJ mol^{-1}	enthalpy ref
allene	−116.3594047	0.0561710[c]	196 ± 5	188 ± 5	4
Cl	−459.6058017[d]		119.62 ± 0.01	121.30 ± 0.01	39
(*E*)−1-chloroallyl radical	−576.0262998	0.0592840	147 ± 7	138 ± 7	4
(*Z*)−1-chloroallyl radical	−576.0270409	0.0595580	145 ± 7	136 ± 7	4
2-chloroallyl radical	−576.0249185	0.0584430	149 ± 7	139 ± 7	4
(*E*)−1-chloro-1-propen-2-yl radical	−575.9915157	0.0594250	246 ± 2	238 ± 2	4
(*Z*)−1-chloro-1-propen-2-yl radical	−575.9945889	0.0606730	238 ± 2	229 ± 2	4
(*E*)−2-chloro-1-propen-1-yl radical			240 ± 14	230 ± 14	this work[e]
(*Z*)−2-chloro-1-propen-1-yl radical			257 ± 14	247 ± 14	this work[e]
3-chloro-1-propen-2-yl radical	−575.9909651	0.0605730	247 ± 5	238 ± 5	4
HCl	−460.2642037	0.0070900	−92.1 ± 0.4	−92.3 ± 0.4	39
propargyl radical	−115.7087396	0.0436430	341 ± 4	339 ± 4	7

[a] 1 hartree = 2625.50 kJ·mol^{-1}. [b] Indicated error is two standard deviations (2σ) and includes systematic errors propagated from the reported measurements. [c] $(H_0^{ZPE})^{QCISD}$ = 0.056039 hartree and $(H_0^{ZPE})^{B3LYP}$ = 0.055137 hartree. [d] A correction of E = −0.0013382 hartree is added to account for the spin−orbit energy. [e] Computed using the G2 energies in ref 40, $\Delta_f H_{298.15}^\circ$(2-chloropropene) = −24.7 kJ·mol^{-1} from ref 41, $\Delta_f H_{298.15}^\circ(C_2H_4)$ from ref 42, $\Delta_f H_{298.15}^\circ(C_2H_3)$ from ref 43, and the isodesmic reaction, (*E*,*Z*)-2-chloro-1-propen-1-yl + C_2H_4 → C_2H_3 + 2-chloropropene.

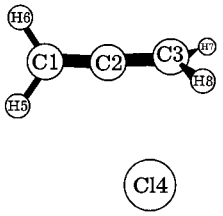

Figure 1. Schematic of the Cl + allene system showing the numbering system of the atoms.

$(H_0^{ZPE})^{MP2}$, the zero point energy correction computed at the MP2/6-31+G(d,p) level, and $\Delta_f H_T^\circ$, the experimentally derived enthalpy of formation. The uncertainty listed with each enthalpy of formation is the error propagated from the underlying, previously reported, thermochemical measurements. Because these errors are presumed to be symmetric about a mean, the listed uncertainties are two standard deviations (2σ). $\Delta_f H_T^\circ$ are used to derive the reaction enthalpies of reactions **1**−**10**, which are presented in the Introduction. The energy diagrams presented in this paper are based solely on ab initio results. To save considerable computational resources, we use $(H_0^{ZPE})^{MP2}$ in derivations $\Delta_{rel}H_0^\circ$ for the persistent species (Table 1). Substitution of $(H_0^{ZPE})^{MP2}$ for $(H_0^{ZPE})^{QCISD}$ (or $(H_0^{ZPE})^{B3LYP}$ for $(H_0^{ZPE})^{QCISD}$) is expected to introduce negligible relative error. The NIST Computational Chemistry Comparison and Benchmark DataBase[32] lists QICSD/6-31G(d), MP2/6-31G(d), and B3LYP/6-31G(d) vibrational frequency data sets for nine chlorinated molecules.[33] The zero point energies computed for these data sets differ by ≈1%.

During this study we found eight transition state structures and one intermediate structure associated with reactions **2**−**7**, all of which exhibit a' symmetry of the C_s point group. Figure 1 displays the atom numbering system used in this paper for geometry descriptions of the transition states and intermediate structures. Supplementary Table 1S lists the fully optimized geometries obtained at the QCISD/6-31+G(d,p) level with reference to the atom numbering system. Transition state geometries obtained at other levels are not reported because these differ only slightly from the QCISD/6-31+G(d,p) structures. Supplementary Table 1S also lists the electronic energy at the highest level of calculation (usually $H^{Q(T)//QCISD}$), H_0^{ZPE}, and the $\nu_i^\ddagger$, the imaginary frequency corresponding to the transition state. Table 2 lists $\Delta_{rel}H_0^{level}$(TS), the energy at 0 K of the transition state relative to the initial reactants, Cl + allene, for up to seven levels of theory. Each $\Delta_{rel}H_0^{MP2}$ entry also lists the spin eigenvalue, $\langle S^2\rangle_o$, evaluated at the fully optimized MP2/6-31+G(d,p) geometry. Each $\Delta_{rel}H_0^{PMP2}$ entry lists the spin eigenvalue, $\langle S^2\rangle_p$, computed at the fully optimized MP2/6-31+G(d,p) geometry after full annihilation of spin contaminants.[15,16,25−28] Table 2 lists ΣAVA, the absolute value average energy difference of the stationary states, $|\Delta_{rel}H^{level} - \Delta_{rel}H^{Q(T)//QCISD}|$, which are summed across each row of Table 2 and divided by m, the number of listed energies. Calculations that did not produce a stationary point are excluded from the computation. ΣAVA provides a measure of the performance of the lower levels of theory used in this work relative to the results computed at the highest level (QCISD(T)/6-311+G(d,p)//QCISD/6-31+G(d,p)).

Metathesis and Addition Channels. Reactions **1**−**3** describe the three outcomes of the initial interaction of a Cl atom with allene. Figure 2 depicts the energy diagram for these reactions at 0 K and summarizes the principal findings of the ab initio calculations. All computational levels found a transition structure for the metathesis reaction **1**. This fully optimized transition structure (TS1) leads to HCl and propargyl radical products through direct abstraction of a hydrogen atom. QCISD(T)/6-311+G(d,p)//QCISD/6-31+G(d,p) calculations find $\Delta_{rel}H_0^{Q(T)//QCISD}$(TS1) = 15 kJ mol^{-1}, indicating that a somewhat sizable barrier impedes direct hydrogen abstraction from allene. As indicated in Figure 2, we found no evidence for energy barriers that would inhibit facile addition of the Cl atom onto the end and center carbons. To examine chlorine addition reactions **2** and **3**, we conducted a series of relaxed potential energy scans at the B3LYP/6-31+G(d,p) and MP2/6-31+G(d,p) levels of theory as a function of carbon−chlorine distance. These scans demonstrated that the relative energy diminishes continuously as the chlorine−carbon internuclear distance decreases from 4 Å to the equilibrium distance (≈1.8 Å). Given that both addition reactions have negligible energy barriers and that metathesis reaction **1** has an energy barrier of approximately 15 kJ·mol^{-1}, we expect chlorine addition to dominate the reactivity at low temperatures. Thus, the incipient products of Cl + allene are ensembles of 3-chloro-1-propen-2-yl and 2-chloroallyl radicals of comparable size.

For completeness, we note that elementary HCl metathesis processes involving 3-, 4-, and 5-center transition structures from the 2-chloroallyl and 3-chloro-1-propen-2-yl radicals may exist. Since preliminary explorations for these transition structures

TABLE 2: Energies of Transition States and Stationary Structures Relative to the Initial Reactants, Cl and C_3H_4, at 0 K

level, kJ mol^{-1}	TS1	TS4a	IS4c	TS4v	TS4r	TS5	TS6	TS7	TS8	ΣAVA,[a] kJ·mol^{-1}
$\Delta_{rel}H_0^{Q(T)//QCISD}$ [b]	15	−9	−7	−15	−94[c]	111[c]	293[c]	118[c]	113[c]	0
$\Delta_{rel}H_0^{Q(T)//MP2}$	26	3	6	−5	−94[d]	*e*	294	*e*	120	3
$\Delta_{rel}H_0^{Q(T)//B3LYP}$	12	−12	*f*	*f*	−100	115	292	121	106	1
$\Delta_{rel}H_0^{QCISD}$ [b]	34	0	−1	−5	−86[c]	132[c]	321[c]	139[c]	138	16
$\Delta_{rel}H_0^{PMP2}$ [g]	13	−4	5	−13	−101	*e*	300	*e*	114	6
	$\langle S^2\rangle_p = 0.76$	$\langle S^2\rangle_p = 0.76$	$\langle S^2\rangle_p = 0.75$	$\langle S^2\rangle_p = 0.78$	$\langle S^2\rangle_p = 0.75$		$\langle S^2\rangle_p = 0.75$		$\langle S^2\rangle_p = 0.77$	
$\Delta_{rel}H_0^{MP2}$	67	22	7	20	−85	*e*	303	*e*	149	23
	$\langle S^2\rangle_o = 1.07$	$\langle S^2\rangle_o = 0.91$	$\langle S^2\rangle_o = 0.76$	$\langle S^2\rangle_o = 0.95$	$\langle S^2\rangle_o = 0.86$		$\langle S^2\rangle_o = 0.77$		$\langle S^2\rangle_o = 0.95$	
$\Delta_{rel}H_0^{B3LYP}$	−20	−38	*f*	*f*	−92	100	296	114	113	15

[a] Average electronic energy difference, $\Sigma AVA = 1/m\sum_{n=TS1}^{n=TS8}|\Delta_{rel}H^{level}(n) - \Delta_{rel}H^{Q(T)//QCISD}(n)|$, where ab initio calculations that have not obtained a stationary structure are not included in each average. The differences do not contain zero point energy contributions. See text. [b] Except as noted, the relative enthalpy contains $(H_0^{ZPE})^{QCISD}$. See text. [c] This reaction enthalpy was computed using $(H_0^{ZPE})^{MP2}$'s evaluated at the corresponding fully optimized MP2/6-31+(d,p) geometries. [d] At Φ = 90° structure. See text. [e] MP2/6-31+G(d,p) structure calculation did not converge to a unique geometry. See text. [f] B3LYP/6-31+G(d,p) calculation found no evidence of a stationary structure. See text. [g] Computed with $H_0^{PMP2} = H^{PMP2} + (H_0^{ZPE})^{MP2}$ evaluated at the fully optimized MP2/6-31+G(d,p) geometry.

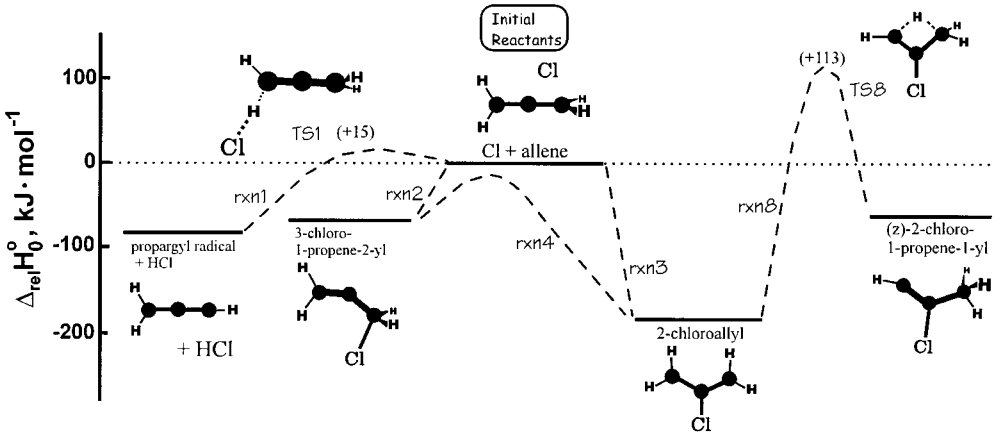

Figure 2. Reaction enthalpy diagram at 0 K of metathesis reaction channels accessible as a chlorine atom approaches allene. Reaction enthalpies are referenced to the reactants (Cl + allene) at 0 K. The values listed in parentheses are the ab initio $\Delta_{rel}H_0^{Q(T)//QCISD}$ (kJ·mol^{-1}) of the transition state structures, which include zero point energy contributions. Dashed lines also show the reaction energy barrier of isomerization reaction 4.

were unsuccessful, exhaustive ab initio searches for these metathesis channels were not pursued.

Isomerization of 3-Chloro-1-propen-2-yl Radicals through Cl Transfer. Ab initio calculations predict that ensembles of 3-chloro-1-propen-2-yl and 2-chloroallyl radicals establish equilibrium fairly rapidly by transferring the chlorine atom between the end and center carbon atoms (reactions **4** and **-4**). Isomerization proceeds through changes along the $\angle Cl^4-C^3-C^2$ coordinate and through rotation about Φ, which is defined as the angle of the C^3H_2 plane relative to the heavy atom plane (i.e., $\Phi \equiv 90° + (\angle C^1-C^2-C^3-H^7 + \angle C^1-C^2-C^3-H^8)/2$). Figure 3a diagrams the energy profile of the 3,2-Cl atom transfer by plotting $\Delta_{path}H^{level}$, the electronic energy relative to Cl + allene, as a function of the $\angle Cl^4-C^3-C^2$ angle. Figure 3b plots $\Delta_{path}H^{level}$ as a function of Φ. The profiles labeled MP2, PMP2, and QCISD were obtained from internal reaction coordinate (IRC) calculations at the MP2/6-31+G(d,p) and QCISD/6-31+G(d,p) theory levels. The profiles labeled QCISD(T) were obtained by rescaling and interpolating the QCISD profiles so that they intersect the $\Delta_{path}H^{Q(T)//QCISD}$ energies computed for each stationary structure. We note that $\Delta_{path}H^{level}$ contains no zero point energy contributions.

A cut on the IRC through dominant coordinate, $\angle(Cl^4-C^3-C^2)$, indicates that the reaction path goes through transition states TS4v and TS4a (Figure 3a) and intersects a third transition state, labeled TS4r, where the reaction path changes over to follow predominantly coordinate Φ (Figure 3b). Starting with the TS4v structure, IRC calculations at the QCISD/6-31+(d,p) and MP2/6-31+(d,p) levels demonstrated that TS4v connects the 3-chloro-1-propen-2-yl radical and the IS4c intermediate structure. Similar IRC calculations demonstrated that TS4a is connected with intermediates IS4c and TS4r. TS4v ($\angle(Cl^4-C^3-C^2) = 97.0°$) resembles the 3-chloro-1-propen-2-yl radical but features a lengthened terminal C−Cl bond ($r(Cl^4-C^3) = 2.4$ Å). IS4c ($\angle(Cl^4-C^3-C^2) = 76.7°$) lies between TS4a and TS4v with the chlorine atom bridging two carbon atoms ($r(Cl^4-C^2) \approx r(Cl^4-C^3) \approx 2.8$ Å). TS4a ($\angle(Cl^4-C^3-C^2) = 62.1°$) features a lengthened chlorine bond at the center carbon ($r(Cl^4-C^2) = 2.4$ Å). The computed spectrum of the IS4c stationary point exhibits positive harmonic vibrational frequencies only, confirming that it is a local energy minimum. TS4r ($\angle Cl^4-C^3-C^2 = 36.4°$) resembles TS4a but is stabilized by a shortened C−Cl bond ($r(C^2-Cl^4) = 1.77$ Å). From TS4r, rotation of the C^3H_2 group from $\Phi = 90°$ to $\Phi = 0°$ provides −65 kJ mol^{-1} of stabilization energy and transforms the C_3H_4Cl complex into the planar 2-chloroallyl radical (Figure 3b). In summary, the IRC calculations show that TS4v, IS4c, TS4a, and TS4r structures reside along a continuous reaction path linking the 3-chloro-1-propenyl and 2-chloroallyl radicals. The lengthened C−Cl bond length and absence of resonance stabilization accounts for the relatively high energies of the TS4v, IS4c, and TS4a stationary structures.

The number of stationary points found along the path of reaction **4** varies with computational level. Calculations at the

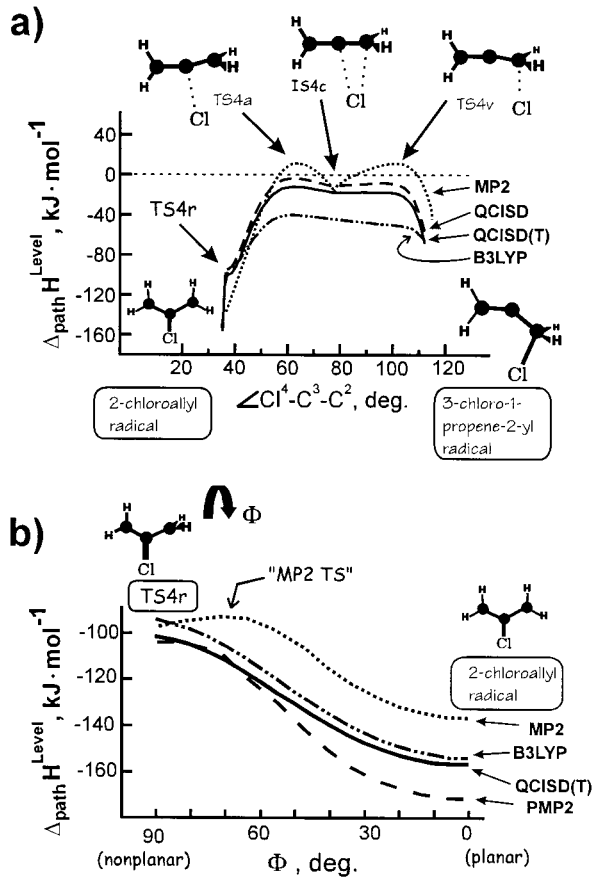

Figure 3. Energy profile governing chlorine atom transfer between the 3-chloro-1-propen-2-yl radical and 2-chloroallyl radical (reaction **4**) predicted by ab initio calculations. Energies are referenced to the separated Cl atom and allene energies at the corresponding computational theory level and do not include zero point energy contributions. (a) Energy profiles as a function of $\angle(Cl^4-C^3-C^2)$. Traces labeled B3LYP, MP2, and QCISD plot $\Delta_{path}H^{B3LYP}$, $\Delta_{path}H^{MP2}$, and $\Delta_{path}H^{QCISD}$, respectively, obtained from IRC calculations with the 6-31+G(d,p) basis set. The trace labeled QCISD(T) is an estimate derived by interpolating the QCISD trace so that it intersects the $\Delta_{path}H^{Q(T)//QCISD}$ computed for each diagrammed structure. (b) Reaction path linking TS4r with the 2-chloroallyl radical plotted as $\Delta_{path}H^{level}$ as a function of Φ, the internal rotation of the CH_2 group plane relative to the plane of the heavy atoms of the C_3H_4Cl radical (See text.).

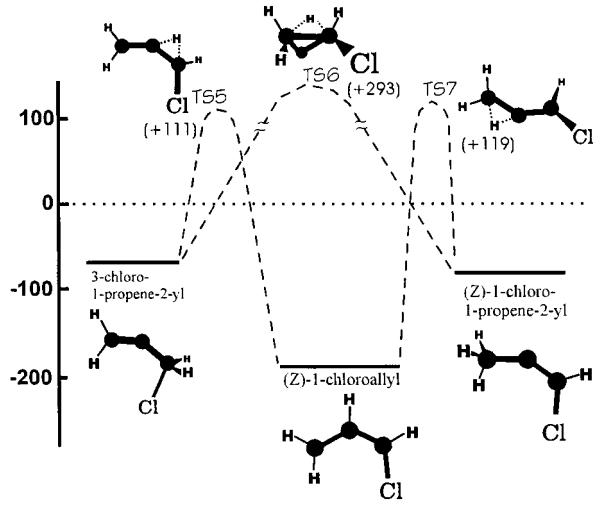

Figure 4. Reaction enthalpy diagram at 0 K showing channels that may deplete the 3-chloro-1-propen-2-yl radical through hydrogen transfer (reactions **5** and **6**) and a channel that converts the 1-chloroallyl radical to the 1-chloro-1-propen-2-yl radical (reaction 7). Reaction enthalpies are referenced to the separated Cl atom and allene at 0 K. The values listed in parentheses are the ab initio $\Delta_{rel}H_0^{Q(T)//QCISD}$ (kJ·mol^{-1}) of the transition state structures, including zero point energy contributions.

B3LYP/6-31+G(d,p) level failed to find the TS4v and IS4c structures even for optimizations initiated at the fully optimized MP2/6-31+G(d,p) or QCISD/6-31+G(d,p) geometries. Moreover, IRC calculations at the B3LYP/6-31+G(d,p) level that followed the reaction path from TS4a (described by increasing $\angle(Cl^4-C^3-C^2)$) terminated at the 3-chloro-1-propen-2-yl radical instead of the expected IS4c intermediate. The inability of B3LYP calculations to predict the existence of the transition structure TS4v, in marked contrast to the MP2 and QCISD calculations, is consistent with previous observations that density functional methodologies tend to underestimate reaction barriers.[34,35] Our second example involves the potential energy along the Φ coordinate (Figure 3b), leading to the isomerization path between TS4r ($\Phi = 90°$) and the 2-chloroallyl radical ($\Phi = 90°$). MP2/6-31+G(d,p) calculations predict an 8 kJ mol^{-1} C^3H_2 rotational barrier (labeled "MP2 TS" in Figure 3b) at $\Phi \approx 71°$. At $\Phi = 90°$ the MP2 calculations predict a stationary structure exhibiting only positive vibrational frequencies. In contrast, the B3LYP and QCISD levels of theory predict that TS4r lies at $\Phi = 90°$ and that the CH_2 group rotates into the heavy atom plane (i.e., $\Phi \rightarrow 0°$) in a barrierless fashion. Spin contamination is the most likely reason for the existence of the small reaction barrier in the MP2/6-31+G(d,p) energy profile. This hypothesis is supported by the fact that a value of $\langle S^2\rangle_o \approx 0.86$ is obtained on the fully optimized structures used to construct the $\Delta_{path}H^{MP2}$ profile in Figure 3b. Full annihilation of the spin contaminants at the PMP2 level of theory gives spin eigenvalues of $\langle S^2\rangle_p \approx 0.76$ (which are close to the ideal 0.75 for doublets). The predicted PMP2 energy profile resembles the QCISD and B3LYP profiles exhibiting a maximum at $\Phi = 90°$ and no barrier for rotation to $\Phi = 0°$ (Figure 3b)

The present ab initio results showing that the 2-chloroallyl and 3-chloro-1-propen-2-yl radicals are linked through a continuous reaction path supplants our earlier report[4] that reaction **2** proceeds through a surface intersection. The earlier misinterpretation of the potential energy surface arose partly because the scans were conducted mainly along the $\angle(C^2-C^3-Cl)$ coordinate and the coupling between the path and the C^3H_2 torsion was not monitored with sufficient detail. In reality, the "surface crossing" proposed in our previous study[4] is a bend in the reaction path near TS4r due to coupling between the Φ (C^3H_2 torsion) and $\angle(C^2-C^3-Cl)$ degrees of freedom.

Isomerization of 3-Chloro-1-propen-2-yl Radicals through H Transfer. Figure 4 summarizes the search for transition states that may deplete the 3-chloro-1-propen-2-yl radical ensemble through hydrogen transfer. Table 2 lists the barriers found at each level of calculation. The intrinsic barriers for hydrogen transfer range between 111 and 293 kJ·mol^{-1}, indicating that isomerization via hydrogen transfer is unimportant at ambient temperature. Transition state structures TS6 and TS7 were found at QCISD/6-31+G(d,p), MP2/6-31+G(d,p), and B3LYP/6-31+G(d,p) levels. TS5 was found only at the B3LYP/6-31+G(d,p) level. To estimate the reaction enthalpy of TS5, we computed the necessary electronic energies at the QCISD(T)/6-311+G(d,p)//B3LYP/6-31+G(d,p) level and zero point energies at the B3LYP/6-31+G(d,p) level. The calculations yielded $\Delta_{rel}H_0^{Q(T)//B3LYP}$(TS5) = 111 kJ·mol^{-1}, indicating that the intrinsic barrier for this process lies above Cl + allene. We note that our attempts to optimize the geometry of TS5 at the MP2 and QCISD levels did not succeed. Since these MP2 and QCISD structure calculations consistently gave nonstationary points with

geometries similar to the B3LYP structure and since additional calculations seemed unlikely to make the relative energy of TS5 exothermic relative to Cl + allene, we did not pursue the MP2 and QCISD geometry optimizations further. The reasons for the odd behaviors during the MP2 and QCISD optimizations of TS5 are not understood, and further studies dealing with this issue are currently underway.

Isomerization of 2-Chloroallyl Radicals through H Transfer. Reactions **8**−**10** comprise a reaction scheme that could enable the 2-chloroallyl radical to isomerize into the more stable 1-chloroallyl radical. Reaction **8**, the first step in the reaction scheme, isomerizes the 2-chloroallyl radical into the 2-chloro-1-propene-1-yl radical through 1,3-transfer of a hydrogen atom. Figure 2 diagrams the predicted transition state structures and reaction enthalpies. All levels of theory predict the energy of TS8 to lie significantly above Cl + allene, $\Delta_{rel}H_0^{Q(T)//QCISD}$(TS8) = 113 kJ·mol^{-1}, making reaction **8** relatively unimportant for chemically activated C_3H_4Cl adducts at lower pressure and temperature. Since reaction **8** is essentially inactive under these conditions, reactions **9** and **10** are also unimportant to the overall reaction mechanism and their geometries were not optimized.

Discussion

Initial Reaction Channels of Cl + Allene. By using the ab initio results to identify the energetically accessible elementary channels of Cl + allene, we can assign the reaction mechanism. At all theory levels, the calculations found no evidence for barriers impeding chloride addition at the end and center carbons. The higher level calculations found a 12−26 kJ·mol^{-1} barrier impeding reaction **1**. These results are in accord with the study by Farrell and Taajtes, who observed the metathesis fraction to increase from <2% to ≈100% of total reactivity as temperature increased from 300 to 800 K. [3]

At 300 K the reaction of Cl + allene forms mainly chemically activated 2-chloroallyl and 3-chloro-1-propen-2-yl radicals. The chemically activated C_3H_4Cl ensemble does not contain other isomers because the governing transition state structures, TS5, TS6, and TS8, lie at energies substantially above the initial reactants. Steric factors, not revealed by the calculations, may cause the incipient C_3H_4Cl ensemble to contain a ratio of 2-chloroallyl and 3-chloro-1-propen-2-yl radicals that is not in thermodynamic equilibrium. Even so, the highest level ab initio calculations indicate that reactions **4** and **−4** will restore thermodynamic equilibrium since the isomerization path between these persistent C_3H_4Cl isomers and through the transition state structures lies below the initial reactants (Figure 2). At equilibrium, the 2-chloroallyl radical should overwhelmingly comprise the C_3H_4Cl ensemble because it is ≈99 kJ·mol^{-1} more stable than the 3-chloro-1-propen-2-yl radical (Table 1). Therefore, the ab initio results confirm that the previously reported ultraviolet spectrum and rate coefficients of Cl + allene originate from the 2-chloroallyl radical.

Energy Barrier Accord as a Function of Theory Level. The mechanism of Cl + allene is based upon the relative energies of the intermediates and transition states predicted by ab initio results at seven levels of theory. Although the intrinsic barriers computed at the B3LYP, MP2, and QCISD levels differ significantly, single point QCISD(T)/6-311+G(d,p) energies computed for these lower level geometries agree closely. In Table 2 this accord is reflected by the small ΣAVA among the $\Delta_{rel}H^{Q(T)//B3LYP}$, $\Delta_{rel}H^{Q(T)//MP2}$, and $\Delta_{rel}H^{Q(T)//QCISD}$ (which do not include zero point energies).

The accord shown by using single point calculations at QCISD(T) on the geometries optimized at lower levels of theory suggests the question: "Does a single factor account for the large improvement in the reaction barriers?" In previous ab initio studies of transition states, investigators have attributed barrier height energy error to (1) an inaccurate transition state geometry, (2) spin contamination of the variational wave function leading to an incorrect energy, (3) incomplete capture of the correlation energy, and (4) an inaccurate calculation of the zero point vibrational energy.[36−38] Because QCISD(T) calculations are sensitive to geometry differences, the accord shown by the small ΣAVA (Table 2) confirms that the fully optimized B3LYP, MP2, and QCISD geometries have no systematic differences; so, we discount geometry as the factor governing energy barrier variations with theory level.

Spin contamination contributes the largest error to the MP2 results. We confirm this by comparing barriers, $\Delta_{rel}H_0^{MP2}$, obtained from spin-unprojected UMP2 wave functions ($\langle S^2\rangle_o$ = 0.86−1.07), with the corresponding barriers, $\Delta_{rel}H_0^{PMP2}$, obtained from UMP2 wave functions corrected by annihilation of spin contaminants ($\langle S^2\rangle_p$ = 0.75−0.78, which are essentially values corresponding to a doublet, $\langle S^2\rangle_p$ = 0.75.). Across the transition states listed in Table 2, these spin-projected $\Delta_{rel}H_0^{PMP2}$ barriers are typically 16−54 kJ·mol^{-1} lower than the corresponding $\Delta_{rel}H_0^{MP2}$ barriers. (Direct comparisons between $\Delta_{rel}H_0^{MP2}$ and $\Delta_{rel}H_0^{PMP2}$ are valid because they share the same $(H_0^{ZPE})^{MP2}$.) Thus, the spin-projected $\Delta_{rel}H_0^{PMP2}$ barriers are in good accord with the barriers obtained at higher theory levels. Spin contamination can alter the energetics of a reaction sufficiently to produce artifacts similar to the "MP2 barrier" in the isomerization path of reaction 4 (Figure 3b). We note that the MP2 method implemented in most available ab initio programs find optimized molecular structures by using energy gradients based on spin-unprojected wave functions. This absence of spin contamination corrections during the calculation of MP2 gradients may account partially for failure of the MP2 method to locate the transition structures TS5 and TS7, which were found at the QCISD level.

The effects of incomplete capture of correlation energy is seen by comparing the $\Delta_{rel}H^{Q(T)//QCISD}$ and $\Delta_{rel}H^{QCISD}$ results (Figure 3). As indicated by the large ΣAVA of 16 kJ·mol^{-1} (Table 2), the QCISD calculations systematically overestimate barriers, indicating the importance of triple excitations within the quadratic configuration interaction formalism. Barriers predicted by the B3LYP/6-31+G(d,p) energies also exhibit a large discrepancy, ΣAVA = 15 kJ·mol^{-1} (Table 2). Moreover, the computed barriers lie significantly lower than those predicted by the $\Delta_{rel}H^{Q(T)//QCISD}$ reference set. The systematic underestimation of reaction barriers by density functional theories is well-known and probably arises from deficiencies in the exchange-correlation functionals. The energy errors of the B3LYP calculation do not seem to affect the optimized transition state structures. This conclusion is supported by the good accord (small ΣAVA) obtained for the computed electronic transition state energies using the QCISD(T)/6-311(d,p) energy found at each B3LYP/6-31+G(d,p) geometry.

Because the QCISD(T) calculations at the QCISD, MP2, and B3LYP geometries give essentially the same energies, the discord among $\Delta_{rel}H_0^{Q(T)//QCISD}$, $\Delta_{rel}H_0^{Q(T)//MP2}$, and $\Delta_{rel}H_0^{Q(T)//B3LYP}$ measures the influence of the zero point energy calculations upon the predicted energy barriers. The magnitude of this discrepancy is best observed for TS1, TS4a, IS4c, and TS4v for which the average ZPE difference is $(H_0^{ZPE})^{MP2} - (H_0^{ZPE})^{QCISD} \approx$ 8 kJ·mol^{-1} (see suplementary material). The larger H_0^{ZPE} obtained at the MP2/6-31+G(d,p) level accounts for the higher barriers predicted by this theory level. The sparse

data available for TS1 and TS4a suggest that the ZPE contributions computed at the B3LYP/6-31+G(d,p) level may agree more closely with the $(H_0^{ZPE})^{QCISD}$ reference. In summary, the QCISD(T)/6-31+G(d,p)//QCISD/6-31+G(d,p) method appears to minimize the errors contributing to transition state energy barriers, lending confidence in the verity of the predicted mechanism for the Cl + allene reaction.

Supporting Information Available: Table 1S lists the fully optimized geometries obtained at the QCISD/6-31+G(d,p) level with reference to the atom numbering system of Figure 1. Table 1S also lists the electronic energy at the highest level of calculation (usually $H^{Q(T)//QCISD}$), H_0^{ZPE}, and the $\nu_i^{\ddagger}$, the imaginary frequency corresponding to the transition state. This material is available free of charge via the Internet at http://pubs.acs.org.

References and Notes

(1) *Chemical Kinetics Database on the Web, Standard Reference Database 17, Version 7.0 (Web Version)*, Public Beta Release 1.0, National Institute of Standards and Technology, http://kinetics.nist.gov, 2001.

(2) Wallington, T. J.; Skewes, L. M.; Siegl, W. O. *J. Photochem. Photobiol. A. Chem.* **1988**, *45*, 167.

(3) Farrell, J. T.; Taatjes, C. A. *J. Phys. Chem. A* **1998**, *102*, 4846.

(4) Atkinson, D. B.; Hudgens, J. W. *J. Phys. Chem. A* **2000**, *104*, 811.

(5) Tsang, W. *Combust. Sci. Technol.* **1990**, *74*, 99.

(6) Tsang, W. *A Pre-processor for the Generation of Chemical Kinetics Data for Simulations*; AAIA-2001-0359, 39th AIAA Aerospace Sciences Meeting and Exhibit, January 8-11, 2001, Reno, NV.

(7) Atkinson, D. B.; Hudgens, J. W. *J. Phys. Chem. A* **1999**, *103*, 7978.

(8) Atkinson, D. B.; Hudgens, J. W. *J. Phys. Chem. A* **1999**, *103*, 4242.

(9) Atkinson, D. B.; Hudgens, J. W. *J. Phys. Chem. A* **1997**, *101*, 3901.

(10) Haszeldine, R. N.; Leedham, K.; Steele, B. R. *J. Chem. Soc.* **1954**, 2040.

(11) Jacobs, T. L.; Illingworth, G. E., Jr. *J. Org. Chem.* **1963**, *28*, 2692.

(12) Griesbaum, K.; Oswald, A. A.; Hall, D. N. *J. Org. Chem.* **1964**, *29*, 2404.

(13) Kovachic, D.; Leitch, L. C. *Can. J. Chem.* **1961**, *39*, 363.

(14) Certain commercial materials and equipment are identified in this paper in order to adequately specify the experimental procedure. Such identification neither implies recommendation or endorsement by the National Institute of Standards and Technology, nor does it imply that the material or equipment identified is the best available for the purpose.

(15) Frisch, M. J.; Trucks, G. W.; Schlegel, H. B.; Scuseria, G. E.; Robb, M. A.; Cheeseman, J. R.; Zakrzewski, V. G.; Montgomery, J. A., Jr.; Stratmann, R. E.; Burant, J. C.; Dapprich, S.; Millam, J. M.; Daniels, A. D.; Kudin, K. N.; Strain, M. C.; Farkas, O.; Tomasi, J.; Barone, V.; Cossi, M.; Cammi, R.; Mennucci, B.; Pomelli, C.; Adamo, C.; Clifford, S.; Ochterski, J.; Petersson, G. A.; Ayala, P. Y.; Cui, Q.; Morokuma, K.; Malick, D. K.; Rabuck, A. D.; Raghavachari, K.; Foresman, J. B.; Cioslowski, J.; Ortiz, J. V.; Stefanov, B. B.; Liu, G.; Liashenko, A.; Piskorz, P.; Komaromi, I.; Gomperts, R.; Martin, R. L.; Fox, D. J.; Keith, T.; Al-Laham, M. A.; Peng, C. Y.; Nanayakkara, A.; Gonzalez, C.; Challacombe, M.; Gill, P. M. W.; Johnson, B. G.; Chen, W.; Wong, M. W.; Andres, J. L.; Head-Gordon, M.; Replogle, E. S.; Pople, J. A. *Gaussian 98*, revision A.7; Gaussian, Inc.: Pittsburgh, PA, 1998.

(16) Frisch, M. J.; Trucks, G. W.; Schlegel, H. B.; Gill, P. M. W.; Johnson, B. G.; Robb, M. A.; Cheeseman, J. R.; Keith, T.; Petersson, G. A.; Montgomery, J. A.; Raghavachari, K.; Al-Laham, M. A.; Zakrzewski, V. G.; Ortiz, J. V.; Foresman, J. B.; Cioslowski, J.; Stefanov, B. B.; Nanayakkara, A.; Challacombe, M.; Peng, C. Y.; Ayala, P. Y.; Chen, W.; Wong, M. W.; Andres, J. L.; Replogle, E. S.; Gomperts, R.; Martin, R. L.; Fox, D. J.; Binkley, J. S.; Defrees, D. J.; Baker, J.; Stewart, J. P.; Head-Gordon, M.; Gonzalez, C.; Pople, J. A. *Gaussian 94*, revision D.4; Gaussian, Inc.: Pittsburgh, PA, 1995.

(17) Møller, C.; Plesset, M. S. *Phys. Rev.* **1968**, *46*, 4852.

(18) Becke, A. D. *J. Chem. Phys*. **1993**, *98*, 5648.

(19) Pople, J. A.; Head-Gordon, M.; Raghavachari, K. *J. Chem. Phys.* **1987**, *87*, 5968.

(20) Hehre, W. J.; Ditchfield, R.; Pople, J. A. *J. Chem. Phys.* **1972**, *56*, 2257.

(21) Hariharan, P. C.; Pople, J. A. *Theo. Chim. Acta* **1973**, *28*, 213.

(22) Frisch, M. J.; Pople, J. A.; Binkley, J. S. *J. Chem. Phys.* **1984**, *80*, 3265.

(23) Ditchfield, R.; Hehre, W. J.; Pople, J. A. *J. Chem. Phys.* **1971**, *54*, 724.

(24) Clark, T.; Chandrasekhar, J.; Spitznagel, G. W.; Schleyer, P. V. R. *J. Comput. Chem.* **1983**, *4*, 294.

(25) Schlegel, H. B. *J. Phys. Chem.* **1988**, *92*, 3075.

(26) Schlegel, H. B. *J. Chem. Phys.* **1986**, *84*, 4530.

(27) Sosa, C.; Schlegel, H. B. *Int. J. Quantum Chem*. **1986**, *29*, 1001.

(28) Sosa, C.; Schlegel, H. B. *Int. J. Quantum Chem*. **1987**, *30*, 155.

(29) Gonzalez, C.; Schlegel, H. B. *J. Chem. Phys.* **1991**, *95*, 5853.

(30) Gonzalez, C.; Schlegel, H. B. *J. Chem. Phys.* **1989**, *90*, 2154.

(31) Gonzalez, C.; Schlegel, H. B. *J. Phys. Chem.* **1990**, *94*, 5523.

(32) *NIST Computational Chemistry Comparison and Benchmark DataBase version 5*, Release 5b, Johnson, R. D., III, Oct 2001, http://srdata.nist.gov/cccbdb.

(33) The scaling factors were derived using the experimentally measured vibrational frequencies of chloroethene, chloroform, ethyl chloride, methyl chloride, methylene chloride, 1,2-dichloroethane, (*E*)-1,2-dichloroethene, (*Z*)-1,2-dichloroethene, and 2-chloropropane listed in ref 32.

(34) Baker, J.; Muir, M.; Andzelm, J.; Scheiner, A. Hybrid Hartree−Fock Density-Functional Theory Functionals: The Adiabatic Connection Methodol. In *Chemical Applications of Density-Functional Theory*; Laird, B. B., Ross, R. B., Ziegler, T., Eds.; American Chemical Society: Washington, DC, 1996; p 342.

(35) Johnson, B. G.; Gonzalez, C.; Gill, P. M. W.; Pople, J. A. *Chem. Phys. Lett.* **1994**, *221*, 100.

(36) Chuang, Y. Y.; Coitino, E. L.; Truhlar, D. G. *J. Phys. Chem. A* **2000**, *104*, 446.

(37) Durant, J. L.; Rohlfing, C. M. *J. Chem. Phys.* **1993**, *98*, 8031.

(38) Durant, J. L. Computational Thermochemistry and Transition States. In *Computational Thermochemistry*; Irikura, K. K., Frurip, D. J., Eds.; American Chemical Society: Washington, DC, 1998; Vol. 677, pp 267−284.

(39) Chase, M. W., Jr.; Davies, C. A.; Downey, J. R., Jr.; Frurip, D. J.; McDonald, R. A.; Syverud, A. N. *J. Phys. Chem. Ref. Data* **1985**, *14*.

(40) For the isogyric calculations we used the values $H_{298.15}^{G2} = -576.118079$ hartree and $H_0^{G2} = -576.123412$ hartree for the (*E*)-2-chloro-1-propen-1-yl radical and $H_{298.15}^{G2} = -576.111574$ hartree and $H_0{}^{G2} = -576.116898$ hartree for the (*E*)-2-chloro-1-propene-1-yl radical. The calculations also use $H_{298.15}^{G2}(C_2H_3) = -77.735768$ hartree, $H_{298.15}^{G2}(C_2H_4) = -78.411941$ hartree, and $H_{298.15}^{G2}$(2-chloropropene) $= -576.797197$ hartree.

(41) Shevtsova, L. A.; Rozhnov, A. M.; Andreevskii, D. N. *Russ. J. Phys. Chem. (Engl. Transl.)* **1970**, *44*, 852−855.

(42) Gurvich, L. V.; Veyts, I. V.; Alcock, C. B. *Thermodynamic Properties of Individual Substances*, 4th ed.; Hemisphere Publishing Corp.: New York, 1991; Vol. 2.

(43) Tsang, W. Heats of Formation of Organic Free Radicals by Kinetic Methods in Energetics of Organic Free Radicals. In *Energetics of Organic Free Radicals*; Simoes, J. A., Greenberg, A., Liebman, J. F., Eds.; Blackie Academic and Professional: London, 1996; pp 22−58.